IRANIAN JOURNAL OF PHYSICS RESEARCH

Iranian Journal of Physics Research, Vol. 18, No. 3, 2018

Frequency–driven chaos in the electrical circuit of Duffing-Holmes oscillator and its control

M D Moinul Islam[1], S Basu[2], D Halder[3], A De[4], and S Bhattacharya[1]
1. Department of Physics, Barasat Govt. College, Kolkata, W.B., India
2. Radiological Physics and Advisory Division, Bhaba Atomic Research Centre, Mumbai, India
3. Department of Physics, Kingston Educational Institute, Kolkata, India
4. Raniganj Girls' College, Raniganj, Burdwan, W.B., India

(Received 26 September 2017 ; in final form 04 December 2017)

Abstract
Accurate detection of weak periodic signals within noise and the possibility of secure messaging have made Duffing oscillator (DO) highly important in the field of communication. Investigation on the properties of DO is, thus, very important. An elegant approach to accomplish this is to fabricate electronic circuit simulating DO non-linear equation and to study the effect of input signal amplitude (V_{in}) and frequency (f), disentangling these two from each other. Recently, V_{in}-driven chaotic dynamics has been studied by constructing a simple Duffing-Holmes (DH) oscillator circuit. However, the f-driven characteristics of the oscillator remain unknown at constant V_{in}. The present work is based on the MATLAB simulation of the f-driven chaotic dynamics of the DH equation. Similar output, mixed with chaos and non-chaos, is obtained by constructing the circuit, both in lab and by PSPICE simulation. The circuit moves into complete chaos at f=270 Hz, while period-2 bifurcation appears at f=680 Hz for the constant V_{in} 0.9V. The chaos control is also achieved by two simple methods. In the first method, the variation of the circuit parameter (capacitance) induces chaos control. In the second one, synchronization is achieved by coupling two similar oscillators. These two methods, though apparently simple, could be highly beneficial for using DH in secure communication.

Keywords: nonlinear dynamics, chaos, Duffing-Holmes oscillator, electronic circuit, MATLAB, PSPICE, chaos control

1. Introduction

Chaos theory is an important branch of science to understand the behavioral dynamics of a complex nonlinear system. It aims at investigating the general order inherent within the disorder and unpredictability of a natural system [1, 3]. A large number of chaotic phenomena in different fields like physics, engineering, mechanics, biology, etc. could be examined in the best way by using different non-autonomous second-order nonlinear oscillators represented by nonlinear differential equations. The Duffing equation characterizes one among the equations containing the cubic non-linearity. The equation reveals itself in many physical as well as biological systems with a wide applicability. It models the various oscillations like those of soft and hard springs in mechanics. The Duffing oscillator (DO) illustrates the remarkable jump phenomenon and other non-linear behaviours that can help to construct the reduced order models of complex mechanical systems ranging from micro to macro scales [4, 5]. The forced Duffing equation also contributes to understanding the quasi-periodic behaviour of Bose-Einstein Condensates in the periodic lattices [6, 7].

Duffing equation plays an important role in the field of electronics and communication. Duffing oscillator, one of the simplest of this kind, has a tremendous potential to detect weak signals in a noisy environment [8]. Besides, the oscillators could well be used in chaos based secure communication systems [9]. The chaos involved in the Duffing equation, while having been extensively studied theoretically, has generally been overlooked in the experimental research work constructing basic non-linear electrical circuits. However, it is important to understand the nature and behavior of this oscillator for the future use in electrical circuit under different conditions. The possibility of

representing the Duffing oscillator with the double well potential, in the form of the modified Duffing-Holmes (DH) oscillator, by using very simple circuits, was recognized in by Tamaševičūitė *et al.* [10]. The nonlinear circuit, in that paper, was found to be continuously changing from the chaotic state to the steady one and vice versa with the increase of the external driving force. Therefore, it was almost impossible to characterize the dynamics expressed by the electrical circuit by the estimation of the Feigenbaum constant and the largest Lyapunov exponent.

The experimental study of the chaotic dynamics of an electrical circuit using the frequency of the signal source as a driver has rarely been pursued in the past. The present work, therefore, investigates the chaotic dynamics of the electrical DH oscillator circuit experimentally, both as a function of driving frequency (input signal frequency) and the strength of the driving force (input signal amplitude). For the proper characterization of chaos, the Feigenbaum constant and the largest Lyapunov exponent of the oscillator have also been calculated, keeping the signal frequency as the varying parameter. However, chaos is usually undesirable in electronics and communication systems, as it restricts the operating range of the systems. Therefore, the control of chaos is highly important.

The demand of chaos control also arises strongly in the case of secure wireless communication [11- 13]. Research work exists in the field of the control of chaos within the domain of the Chua's circuit [14]. However, there are very few results on chaos control in nonlinear oscillators like DH [15]. Unfortunately, the implementation of chaos control and synchronization, directly in terms of the electric circuit, is rarely studied in the past [16]. In this paper, chaos control is achieved by two different simple methods implemented directly in the electric circuit. The first method changes the magnitude of one of the circuit components. The second one, which is shown here, acts by coupling two similar chaotic oscillators producing the synchronized and stable output. The usage of the DH Oscillator in secure communication can be immensely beneficial with the two synchronization or chaos control methods.

2. The theoretical analysis

The Duffing-Holmes nonlinearity of second order is written as two equivalent sets of non-autonomous differential equations, as can be seen here:

$$\dot{x} = y\,, \tag{1}$$

$$\dot{y} = x - x^3 - ay + b\sin\omega t\,, \tag{2}$$

where x-x^3 is the form of the restoring force $F(x)$. The equations (1) and (2), in combination, represent an externally driven particle in a double-well non-parabolic potential $V(x)$ that can be calculated by integrating the force field $F(x)$ with respect to *x. a, b* and *ω, which* are the damping constant, the forcing amplitude and the forcing frequency, respectively.

2. 2. Numerical calculation using MATLAB

Among the three parameters b, ω and a, which are involved in the equations (1) and (2), the first two parameters were varied in MATLAB to find x and y numerically.

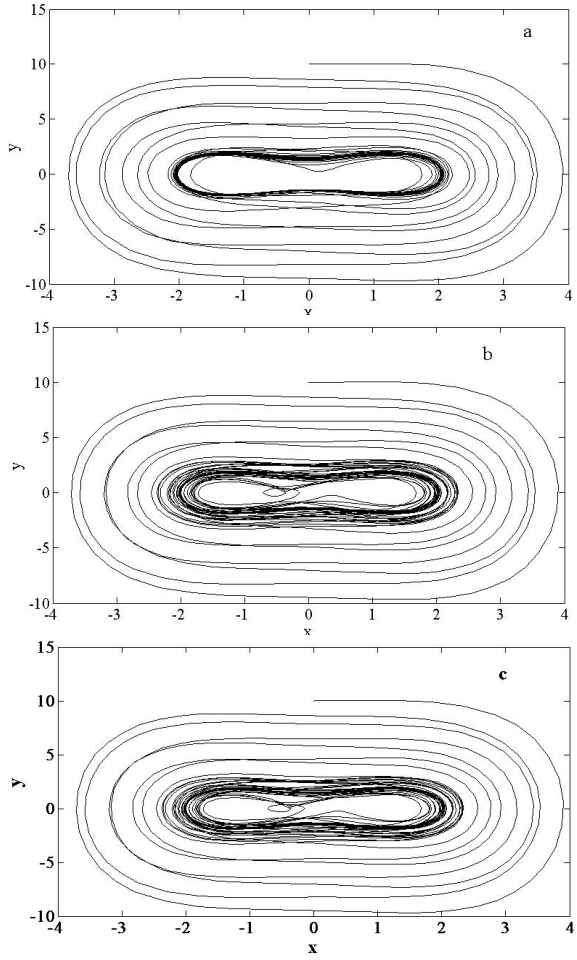

Figure 1. The MATLAB generated the driving force amplitude dependence phase space plot by keeping the frequency constant; (a) ω=1.119, b=1.1, a=0.087; (b) ω=1.119, b=0.9, a=0.087; (c) ω=1.119, b=0.12, a=0.087. Symbols are used as described in the text.

2.2 Dependence on the amplitude (*b*) of the external driving force

Figure 1 (a) to (c) describes how the system moves from the steady state to the chaotic one gradually with the driving force amplitude, under fixed frequency.

2. 3. Dependence on frequency

Variation of the angular frequency ω with the constant amplitude of the driving force results in the variation of the phase space plot; also, it reveals the periodic and chaotic behaviours of the oscillator. The ω-driven phase space dynamics is found to be an ensemble of chaotic and non-chaotic (periodic) modes. The frequency-varied response of the equations (1) and (2) is shown in figure 2 (a) to (f). Among the three parameters b, ω and a ,which are involved in the equations (1) and (2), the first two oes were varied using the MATLAB to find the results in terms of x and y numerically.

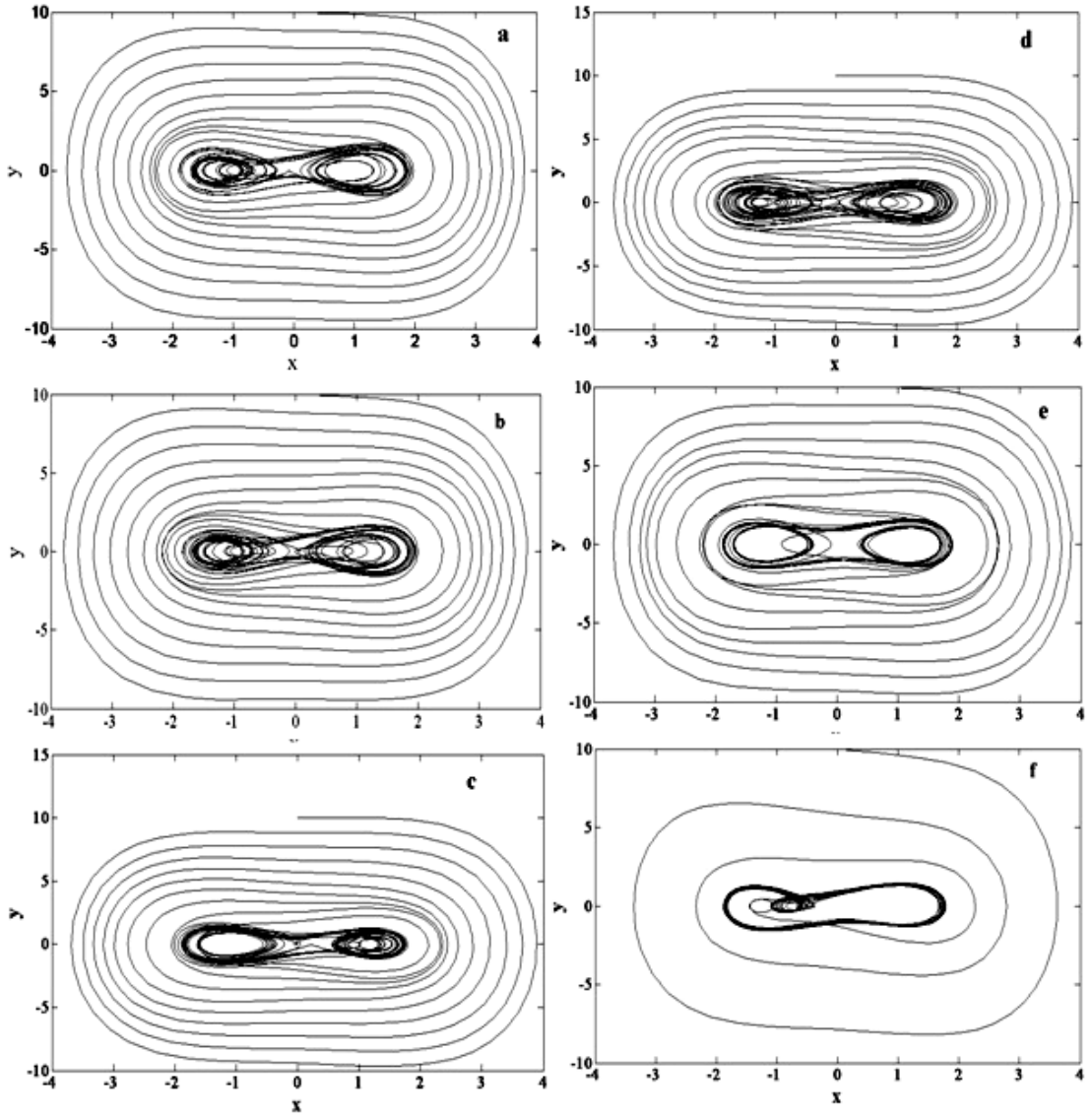

Figure 2. The MATLAB generated variation of the phase space plot with the frequency of the driving force. (a) ω=0.193, b=0.9, a=0.087; (b) ω=0.201, b=0.9, a=0.087; (c) ω=0.231, b=0.9, a=0.087; (d) ω=0.298, b=0.9, a=0.087; (e) ω=0.440, b=0.9, a=0.087; (f) ω=0.507, b=0.9, a=0.087. Symbols are used as described in the text.

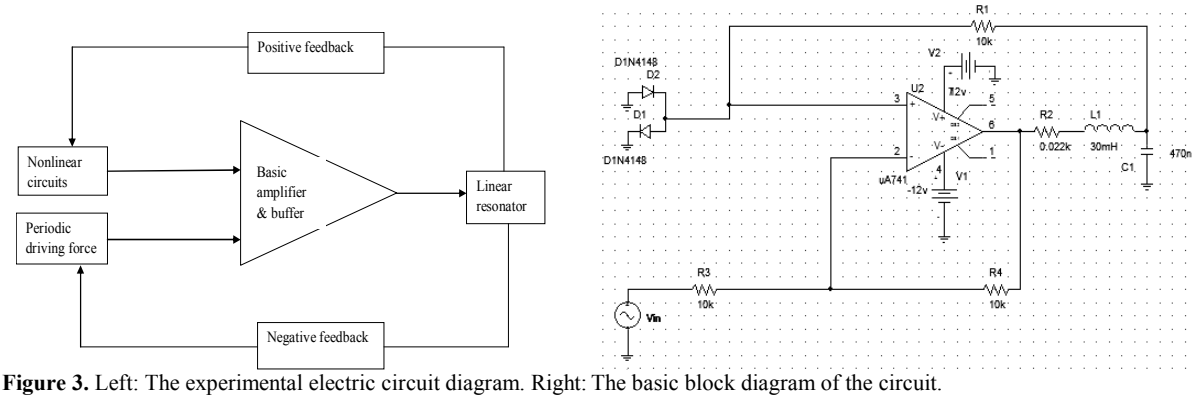

Figure 3. Left: The experimental electric circuit diagram. Right: The basic block diagram of the circuit.

3. The experimental analysis

3.1. Function of the circuit

The circuit, primarily R-L-C one, is shown in the left panel of figure 3 as adopted in [9]. The nonlinear elements in the circuit are R_1 and the p-n junction diodes D_1 and D_2. The op-amp acts as an amplifier in the

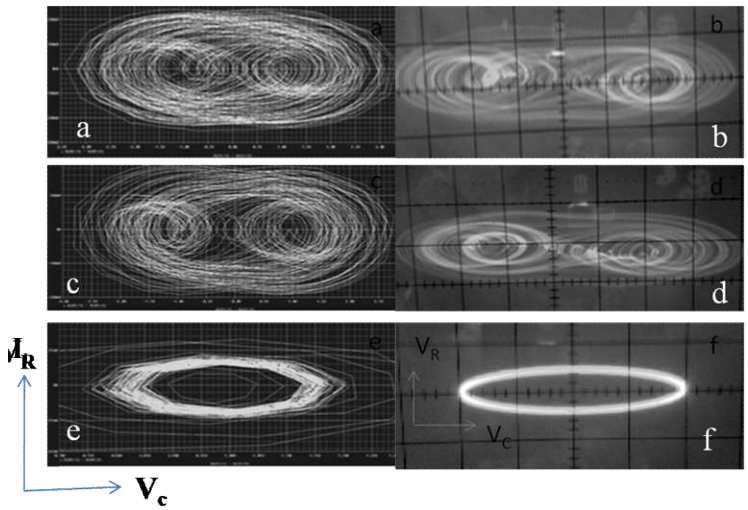

Figure 4. Amplitude-driven dynamics of the electrical circuit. Left panels: (a), (c) and e are I_L vs V_C phase space PSPICE simulations for the circuit parameters b=1.1 and f=1.5kHz (analogous to figure 1 (a)), b=0.9 and f=1.5 kHz (analogous to figure 1 (b)), and b=0.12 and f=1.5 kHz (analogous to figure 1(c)), respectively. Right panels b, d and f are I_L vs V_C phase space experimental data taken from CRO for the circuit parameters b=1.1 and f=1.5 kHz, b=0.9 and f=1.5 kHz and b=0.12 and f=1.5 kHz, respectively. Symbols used are as explained in the text.

nonlinear positive feedback loop as well as a unity gain buffer for the external sinusoidal signal (if R_3 and R_4 are kept the same). The required nonlinearity is introduced in the positive feedback loop of the op-amp by these diodes and resistance. The input sinusoidal signal (periodic driving force) is introduced to the output of the op-amp using it as the unity gain buffer. Thus, the op-amp acts both as a positive and negative feedback nonlinear amplifier. R_2, L_1 and C_1 constitute the linear resonator creating oscillation whose damping is prevented by the op-amp. The oscillator, in combination with diodes and R_2, produces nonlinear oscillation. The basic block diagram of the circuit is also shown in the right panel of figure 3.

Mathematically, the differential equations describing the circuit are given by:

$$C_1 \frac{dV_c}{dt} = I_L , \tag{3}$$

$$L_1 \frac{dI_L}{dt} = f(V_c) - I_L R_2 + A\sin(\omega t - \pi), \tag{4}$$

V_c and I_L are the voltage across the capacitor C_1 and current through the inductor L_1, respectively. The non-linear function $f(V)$ arising out of the diodes is expressed by the following three-segment linear approximation:

$$\begin{aligned} f(V_c) &= -\left[V_c + \left(1+\frac{R_4}{R_3}\right)V_{\text{cut}}\right] \quad , \quad V_c < -V_{\text{cut}} \\ &= \left(\frac{R_4}{R_3} - 1\right)V_c \quad , \quad -V_{\text{cut}} \le V_c \le V_{\text{cut}} \\ &= -\left[V_c - \left(\frac{R_4}{R_3}\right)V_{\text{cut}}\right] \quad , \quad V_c > V_{\text{cut}} \end{aligned} \tag{5}$$

V_{cut} =0.5 V at 0.1 mA is the cutin voltage drop across an the opened diode. Here, we assume $R_1 > \rho = \sqrt{(L_1/C_1)}$. By assuming $x = \frac{V_c}{2V_{\text{cut}}}$, $y = \frac{\rho I_L}{2V_{\text{cut}}}$, $b = \frac{A}{2V_{\text{cut}}}$, $a = \frac{R_2}{\rho}$, $\rho = \sqrt{\frac{L_1}{C_1}}$ =252Ω and taking $\frac{t}{\sqrt{L_1 C_1}} \to t$, $\omega\sqrt{L_1 C_1} \to \omega$, the following equations can be framed for the comparison with the numerical calculations.

$$\dot{x} = y \tag{6}$$

$$y = f(x) - ay + b\sin\omega t \tag{7}$$

where the non-linear function $f(x)$ is given by,

$$\begin{aligned} f(x) &= -(x+1) \quad , \quad x < -0.5, \\ &= x \quad , \quad -0.5 \le x \le 0.5 \\ &= -(x-1) \quad , \quad x > 0.5 \end{aligned} \tag{8}$$

Thus, the equations (6) and (7) are analogous to the equations (1) and (2). But the form of the non-linear function $f(x)$ and hence, the experimental double-well potential (piecewise parabolic) can be different from the theoretical one, though at smaller x –values, they are very similar. The values of the

Circuit parameters are shown in the figure 3. We take the op-amp as IC 741. Figures 4 (a), (c) and (e) display the results of PSPICE simulations and figures 4 (b), (d), (f) depict the experimental data of I_L against V_C in the form of a Lissajous figure photographed from the CRO directly. The results have been obtained by varying the external signal amplitude and keeping the frequency constant. The corresponding values of signal frequency and the input amplitude are also represented.

Figures 5 (a) to (e) show the frequency driven phase space plot from both direct experimental data and PSPICE simulation. The left side figure panels represent the experimental data and right side ones are from PSPICE simulations. The relevant parameters involving the data are described in the same figure.

The experimental results photographed from CRO and the simulated data were found to be in agreement with the numerical results obtained by using MATLAB figures 2 and 5 corroborate each other in terms of

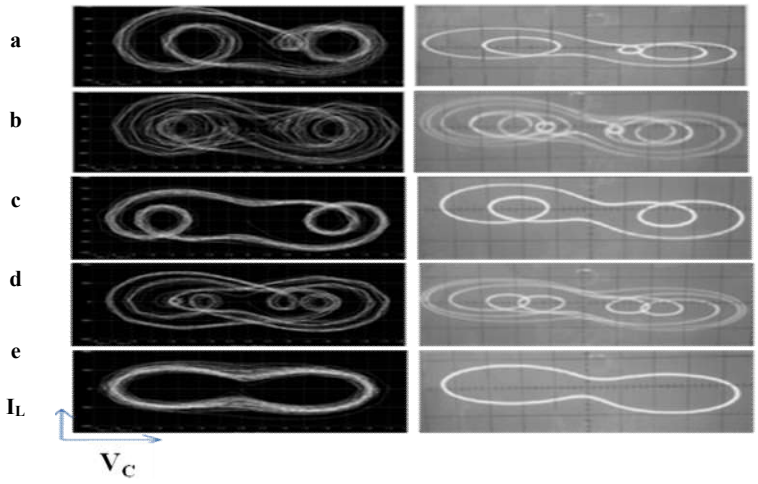

Figure 5. Frequency-driven dynamics (*IL-VC* plot) of the electrical circuit. The left panels are PSPICE simulation and the right ones are the experimental data. Panel (a) Vin=0.9V, f=260Hz (analogous to figure 2 (a)); (b) Vin =0.9V, f=270Hz (analogous to figure 2 (b)); (c) Vin=0.9V, f=310Hz (analogous to figure 2 c); (d) V_{in}=0.9V, f=400Hz (analogous to figure 2 (d)); (e) V_{in} =0.9V, f=680Hz (analogous to figure 2 (f). The figures show the interspersing of chaotic and non-chaotic dynamics. Symbols used are as explained in the text.

frequency variation, while figures 1 and 4 conform to each other in terms of the input driving amplitude). The experimental data along with simulation both confirm that the variation of frequency of the driving voltage can produce an ensemble of chaotic phase space interspersed with non-chaotic and periodic phase spaces.

4. Results and discussion

4. 1. Feigenbaum constant

We estimated the Feigenbaum constant from the frequency driven experimental data using the DH oscillator circuit. The estimation of this constant from the measured data is highly important to understand the chaotic dynamics of the oscillator. It was found that the circuit showed period-2 bifurcation starting from the frequency 680Hz up to 1100 Hz. The period-8 bifurcation could be seen from the frequency 400 Hz to 680Hz, while the period-4 was observed from 310 Hz to 400Hz. By lowering the frequency from 310 Hz to 270Hz, the circuit showed a chaotic behaviour. By lowering further to 260Hz, it gradually moved to the non-chaotic phase.

The Feigenbaum constant [17] is calculated as,

$$\delta = \frac{\text{period4} - \text{period2}}{\text{period8} - \text{period4}} = \left| \frac{310\text{Hz} - 680\text{Hz}}{400\text{Hz} - 310\text{Hz}} \right| = 4.11 \qquad (9)$$

The value of the constant, being 4.11, signals the onset of chaos in the oscillator output.

4. 2. Power spectra and estimation of Lyapunov exponent

To confirm the chaotic nature of the oscillator, the largest Lyapunov exponent (LLE) has been calculated using Wolf's algorithm [18] and the equation (3). The corresponding figures are also mentioned in this table. As it is well-known, the positive LLE signals chaos and the negative LLE represents the non-chaotic phases.

The time response (time vs V_c) of the circuit is shown in figures 6 and 7 for bifurcation and non-chaotic dynamics, respectively. The left side of each of the figures shows the simulated result and the right one represents the results directly photographed from the CRO. The values of LLE for the response shown in figures 6 and 7 were 0.006 and -0.15, respectively, thereby indicating chaotic and non-chaotic phases. The experimental output shown in figure 6 corroborated the output generated (figure 8) from MATLAB under similar conditions. Similarly, MATLAB generated output in figure 9, confirming that shown in figure 7 under the same experimental conditions.

The input frequency driven chaotic dynamics shown in figure 5 is described in table 1 in terms of LLE, input amplitude, frequencies, *a* and *b*. The period-4 bifurcation, related with very low LLE (0.009), was surprising. However, it could be due to the fluctuations in the time series data from which LLE was calculated. Therefore, to confirm the chaotic dynamics, in addition to the LLE, the power spectra were also calculated, as shown in figure 9.

4. 3. Control of chaos

The theoretical concept of oscillator synchronization came from the idea of Pecora and Carroll [12]. Besides, some other theoretical references are also available on oscillator synchronizations [19-21]. However, experimental references are rarely found. Here chaos control in DH oscillator is achieved using two different methods of synchronization with direct realization in the electric circuits.

a. Method 1

The first method of chaos control depends on the variation of the circuit capacitor C_1. The variation in C_1 modifies I_L, which, in turn, changes the chaotic dynamics. The circuit diagram is shown in figure 10, where the capacitor C_1 is changed by placing another capacitor C in parallel. The chaos can be controlled if the

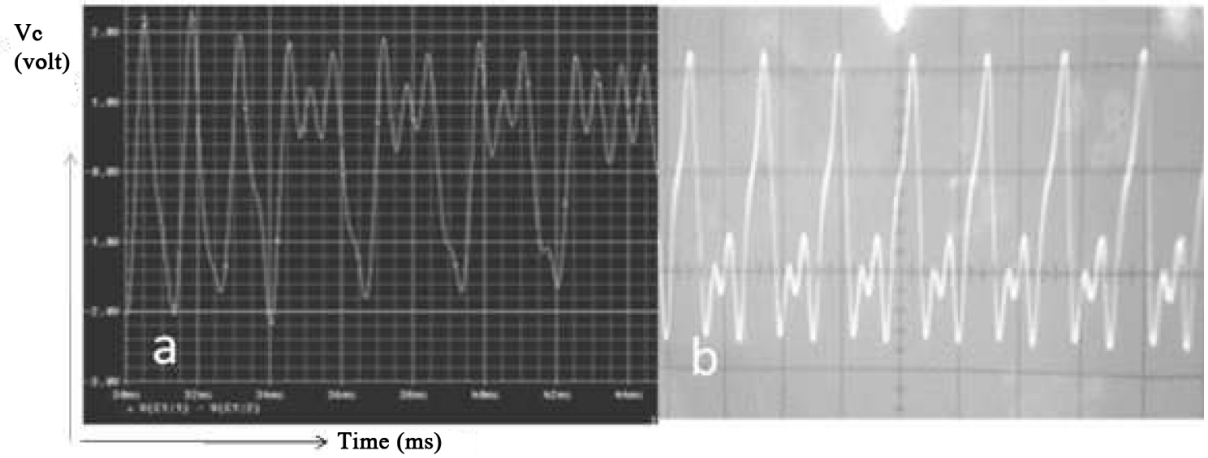

Figure 6. Chaotic time response of V_C. Panel a: PSPICE simulation. Panel (b) Experimental data.

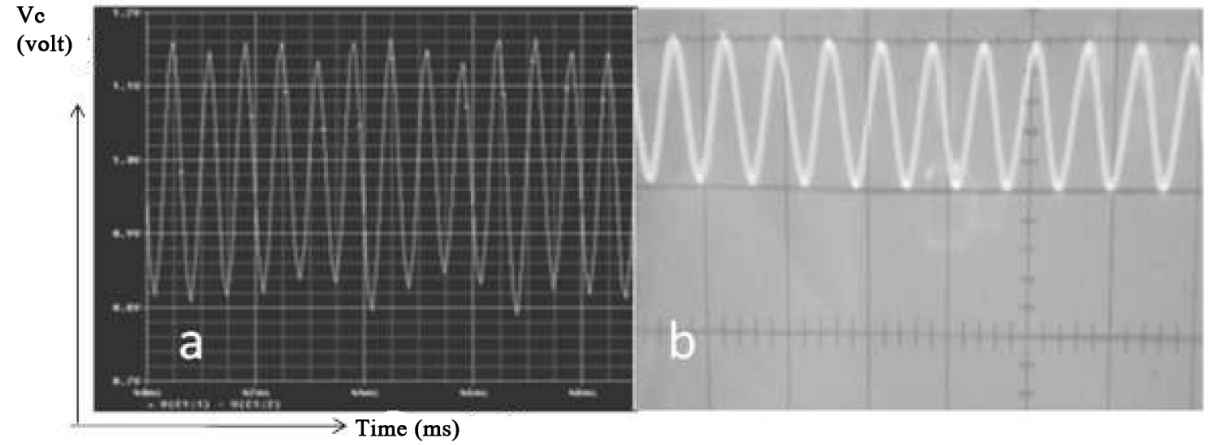

Figure 7. Time response of V_C giving the demise of chaos. Panel (a) PSPICE simulation. Panel (b) Experimental data.

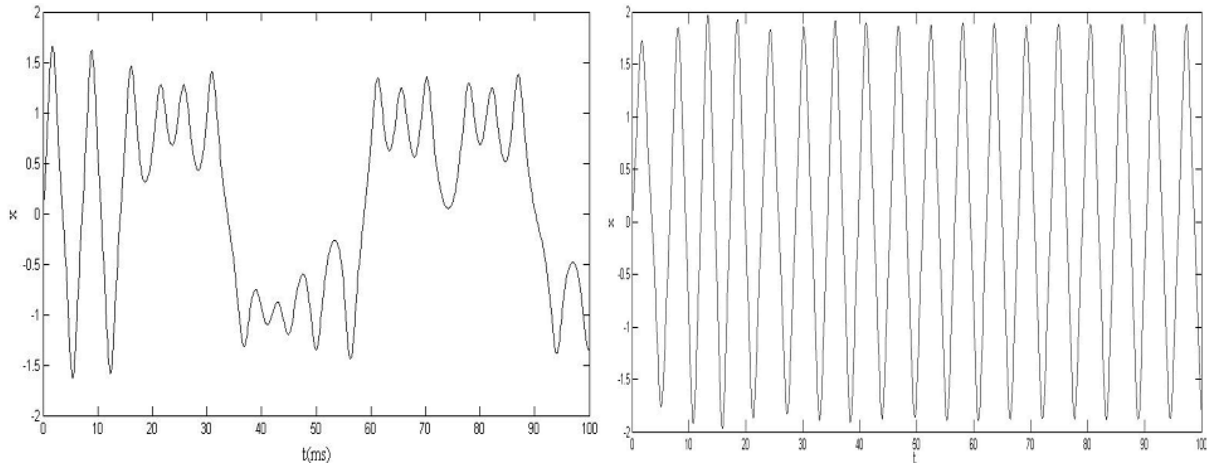

Figure 8. (left) Time response of the bifurcation phase of the DH differential equation solution of x in MATLAB for a=0.087, b=0.9 and ω=1.119, under similar conditions of Figure 6. (right) Time response of x within the non-chaotic phase of DH differential equations solved by MATLAB for a=0.087, b=1.1, ω=1.119, under similar conditions as in Figure 7. Symbols are used as described in the text.

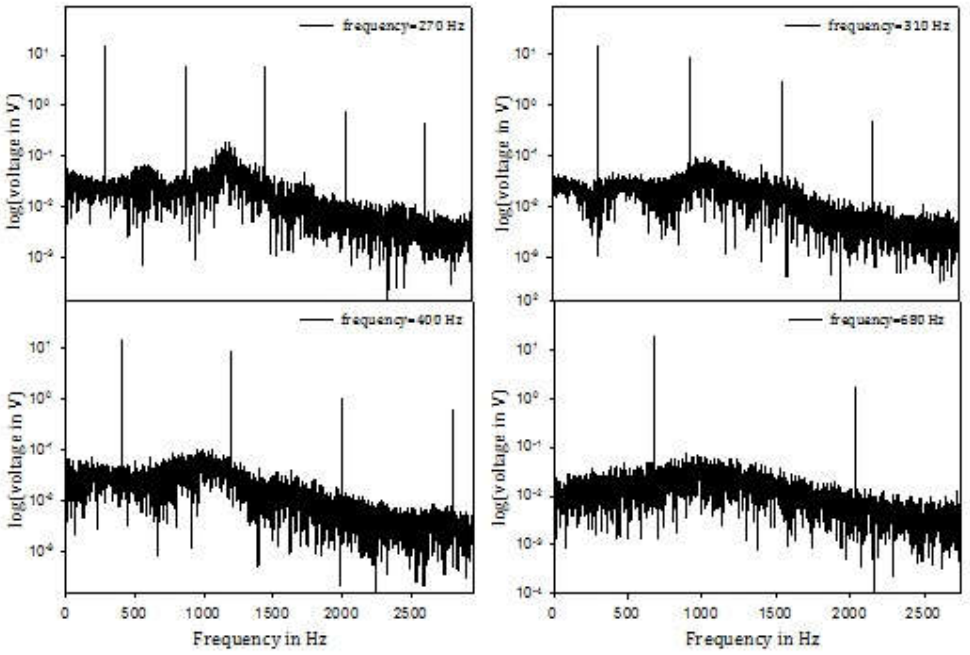

Figure 9. The input frequency driven power spectra of the DH oscillator circuit. *f*=270 Hz gives chaotic spectra. *f*=310Hz and 400 Hz show period 4 bifurcations, while *f*=680Hz is the period-2 only. The details are given in table 1.

Table 1. Characteristics of the observed chaos and the parameters involved.

Exp. Freq. (*f*) Hz.	Input amplitude (V_{in}) Volt	Theo. freq. ω	*a*	*B*	Lyap. Expo. (λ) /power spectra	Figure as displayed in the text	Comment
270	0.9	0.193	0.087	0.9	.026/ figure 9 (a)	figure 5 (b)	chaos
310	0.9	0.230	0.087	0.9	.009/ figure 9 (b)	figure 5 (c)	route to chaos period 4
400	0.9	0.298	0.087	0.9	.030/ figure 9 (c)	figure 5 (d)	route to chaos period 4
680	0.9	0.504	0.087	0.9	-.120/ figure 9d	figure 5 (e)	route to chaos period-2

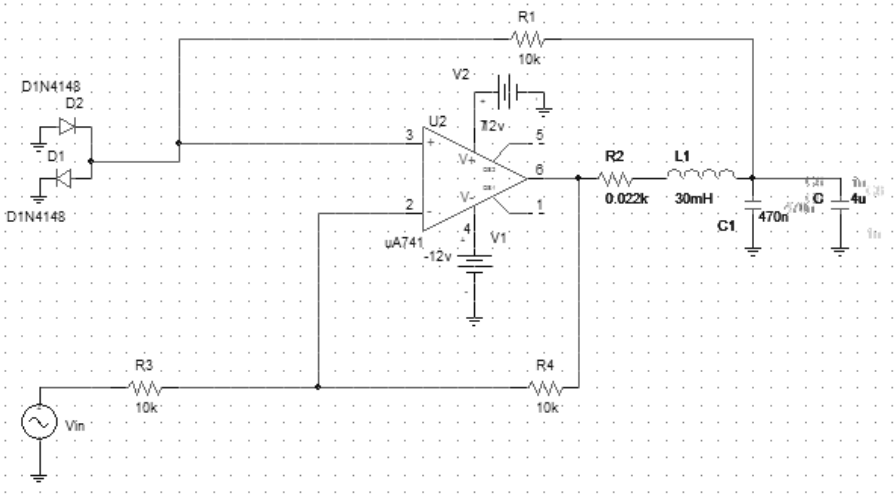

Figure 10. Circuit diagram for chaos control in the DH oscillator. Required change in capacitance is incorporated by putting C in parallel with C_1.

capacitance C is kept within the range 0.2 μF to 4 μF. Thereafter, the increase of C gradually initiates the demise of chaos and again from C= 10 μF onwards, the non-chaotic regions commence. The corresponding

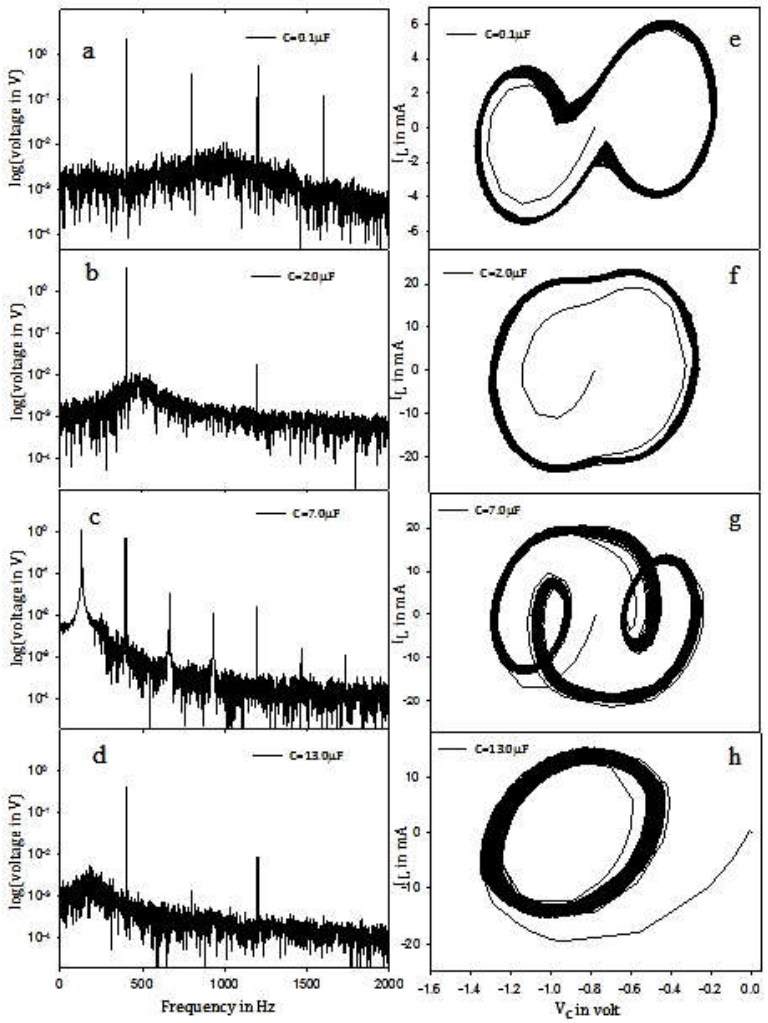

Figure 11. Power spectra and phase space diagrams varying the capacitance C (for V_{in}=0.9V, f=400Hz) of the oscillator. Left (a)-(d) panels are the spectra for C =0.1, 2.0, 7.0 and 13.0 μF, respectively. Right panels (e-h) are the corresponding phase space (I_L-V_C) plots.

power spectra and phase space diagrams are shown in figure 11. Panels a and e in figure 11 give the power spectra and phase space plots (I_L vs V_C) for C are equal to 0.1 μF. The period 2 bifurcation is evident from the phase space plot and can also be corroborated by the two-component (480 Hz and 1200 Hz) power spectra. The other two peaks were simply the mirror images of the two fundamentals. The demise of chaos was evident for C= 2 μF, as shown in the lower background single component peaked power spectra (figure 11 (b)) and the non-bifurcated phase space plot (figure 11 (f)). The component at 1200 Hz dies out. The chaotic dynamics return back again as C is increased to 4μF. The phase space plot given in figure 11 (g) and the power spectra in figure 11c show the data for C=7 μF. The narrow peak at 480 Hz was divided into two broad width sub-components. Similarly, the peak at 1200 Hz was divided into two harmonics. In addition, the power spectrum was contaminated with large background signaling the onset of chaos. The corresponding phase plot giving period-4 bifurcation agreed well with the dynamics. As C was increased, chaos was controlled. Figures 11 (d) and (h) show chaos controlled output. To substantiate the chaosand its control, the bifurcation plot is shown in the left panel of figure 12 for the input driving frequency of 400 Hz and the driving amplitude of 0.9 V, keeping capacitance C as the parameter. If the input frequency is lowered, the chaotic and non-chaotic regimes are repeated again, but with different capacitance values (C). The right panel of figure 12 is the bifurcation plot for the input driving frequency of 270 Hz and the driving amplitude of 0.9 V, with the similar chaotic and non-chaotic regimes but C values different from those given in the left panel of figure 12.

b. Method 2

The second method of chaos control is based on the principle of coupling or synchronization of two similar oscillators. The left panel of figure 13 is the electrical circuit showing the coupled nonlinear oscillators. The output of the second oscillator is connected to the non-inverting input of the op-amp in the first oscillator circuit for synchronization through the black dashed box shown in the figure. The right panel of figure 13 is the basic

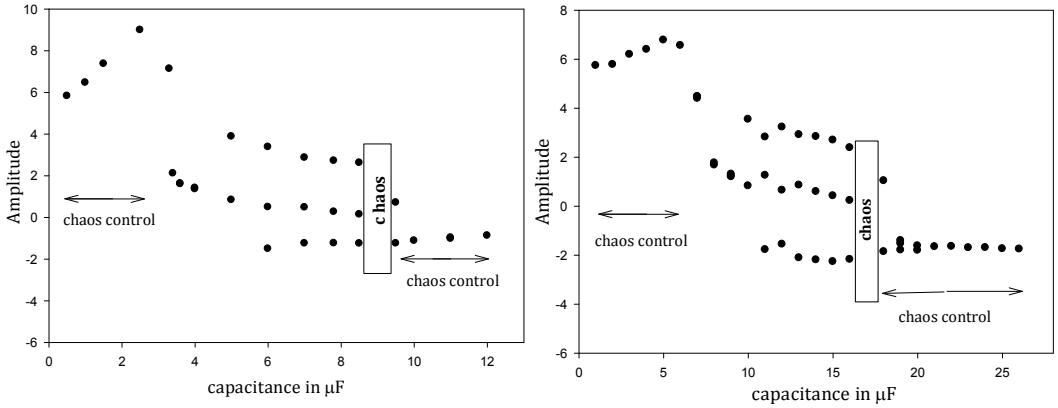

Figure 12. (left) Bifurcation diagram for the frequency f= 400Hz and V_{in}=0.9V of the oscillator, showing chaos control regions and the highly chaotic region. (right) Bifurcation diagram for the frequency of 270Hz and V_{in}=0.9V of the oscillator, showing chaos controlled regions and the highly chaotic region.

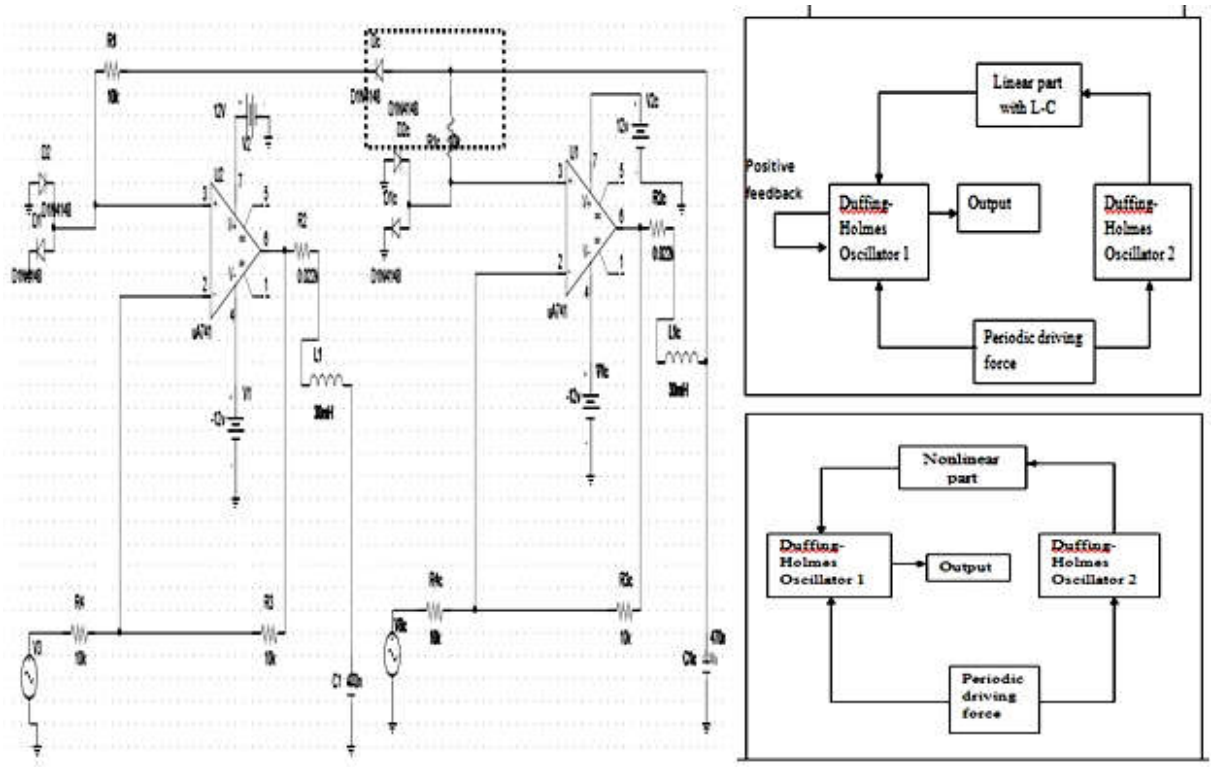

Figure 13. (left) The coupled oscillator circuit to control chaos. Parameters with suffix c denote the second DH oscillator. The dashed box includes the coupling nonlinear part (made by diode) which synchronizes the first DH by modifying the nature of nonlinearity. One can put L-C circuit instead of the nonlinear diodes in the dashed box that will destroy chaos by involving the phase changes. (right top) The basic block diagram of the synchronization with the linear L-C circuit. (right bottom) The basic block diagram of the synchronization with the nonlinear diode circuit.

block diagram of the synchronized circuits. The nonlinear/linear part is the circuit which reduces or removes the chaos. We have used a diode as the nonlinear part which mixes the nonlinearity of different natures in the input of the first DH oscillator. This results in the demise of chaos in the output (the right bottom panel of figure 13). Instead of the nonlinear circuit, linear circuit combination of L-C can also be used to destroy the chaos of first DH by involving the changes in phase (the right top panel of figure 13). In this case, a positive feedback loop is also required to be connected from the output to input of the first DH oscillator.

If the ac input voltage (V_{3c}) of the second i.e coupling oscillator is kept more than 0.2V, the first oscillator moves to chaos. To show the control of chaos, at first, the initial oscillator input voltage V_{in} is fixed at 0.9 V and the input frequency is taken as 500 Hz. At these values, the oscillator output is chaotic. Now, the second oscillator of similar parameters is coupled to the first one as shown in figure 14. The input frequency of the

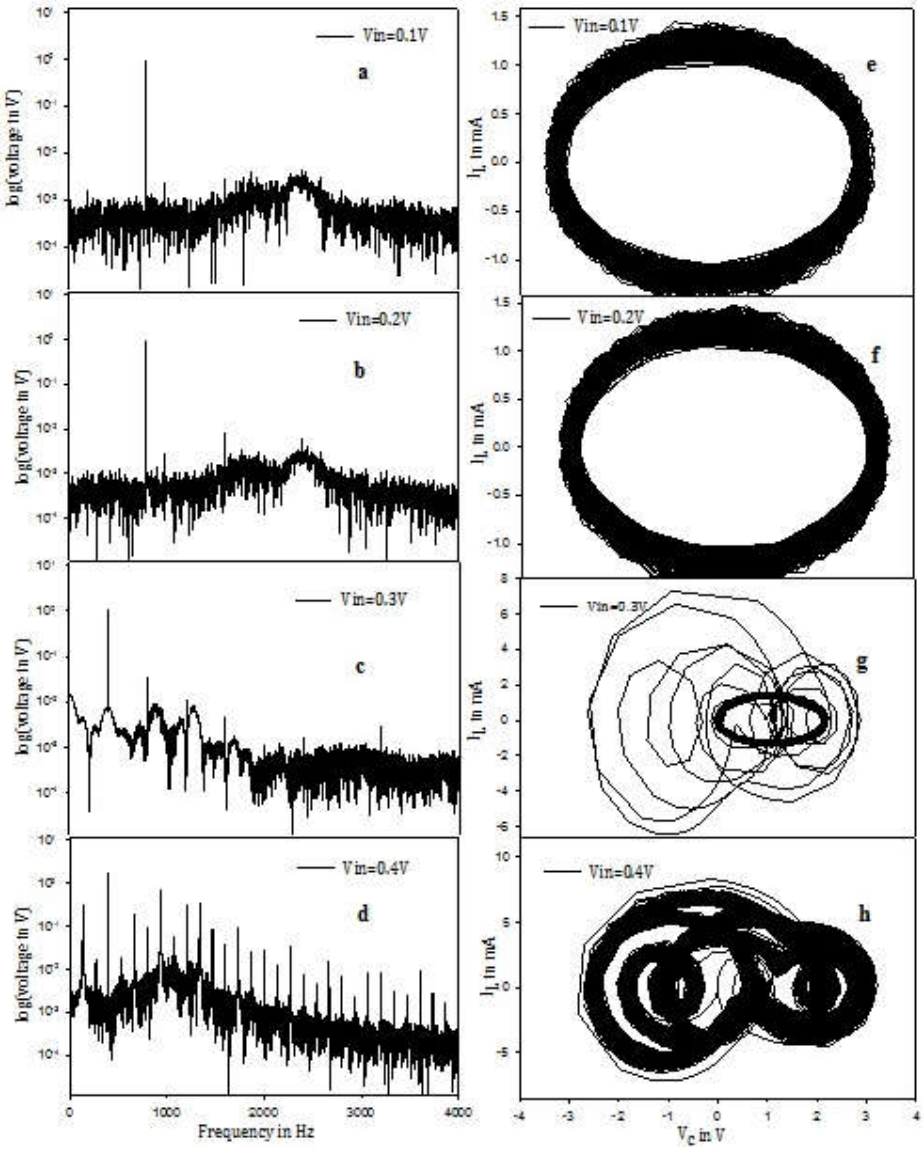

Figure 14. Power spectra and phase space diagrams for the synchronized oscillator circuit, as shown in Figure 14. Left (a)-(d) panels are the power spectra for the input voltage of the second oscillator, i.e V_{3c}=0.1, 0.2, 0.3 and 0.4 V, respectively. Right panels (e-h) are the corresponding phase space (I_L-V_C) plots.

coupling oscillator is also taken as 500 Hz. However, the input voltage is varied. At V_{3c}=0.4 V, the output of the first oscillator is found to be highly chaotic. For V_{3c}=0.3 V, the output is found to be gradually moving towards the non-chaotic phase. Below V_{3c}=0.3 V, the output is completely non-chaotic, making the coupled oscillators synchronized. Similarly, for V_{3c} more than 0.9V, the chaos of first oscillator is destroyed. The chaos control is evident from the power spectra and phase space plots shown in figure 14.

5. Conclusion

As the conclusion, the frequency dependent chaotic behaviour of a very simple DH oscillator circuit was investigated in this work. A collection of intermixed phase space was observed which was a typical characteristic of this circuit.

Here, the Feigenbaum constant was estimated from the experimental data and chaotic dynamics was corroborated by the value of the constant. Wolf's algorithm was used to estimate the largest Lyapunov exponent of a non-linear circuit. The amplitude driven behaviour of the circuit was also studied in detail. The numerical calculation using MATLAB was matched well with the PSPICE simulation and the experimental data.

The chaos in the DH oscillator has also been controlled in two simple ways. By varying one of the circuit parameters, chaos was efficiently controlled. In addition, by coupling two similar DH oscillators, the chaos was controlled by synchronizing both oscillators. The bifurcation diagram, power spectra and phase space plots confirmed the chaos control procedures.

References

1. R C Hilborn, "*Chaos and Nonlinear Dynamics*: *An Introduction for Scientists and Engineers*", 2nd Ed, Oxford University Press (2001).
2. E N Lorenz, *J. Atmos. Sci.* **20** (1963) 130-141.
3. S H Strogatz, "*Nonlinear Dynamics and Chaos*", Perseus Books Publishing: Cambridge, MA (2000).
4. S W Shaw and B Balachandran, *J. Sys. Des. Dyn.* **2** (2008) 611.
5. R Lifshitz and M C Cross, "*Nonlinear Dynamics of Nanomechanical and Micromechanical Resonators*", Eds. G Radons, B Rumpf, and H G Schuster Wiley-VCH, Weinheim (2010).
6. M van Noort, M A Porter, Y Yi, and S N Chow, *J. Nonlinear Saiens* **17**, 1 (2007) 59.
7. V P Chua and A P Mason, *Int. J. Bif. Chaos.* **16** (2006) 945.
8. R Almog, S Zaitsev, O Shtempluck, and E Bucks, *App. Phys. Lett.* **90** (2007) 013508.
9. W Song, D Shen, Y Jianguo, and C Qiang, *Math. Prob. Eng*. **2008** (2008) 1.
10. E Tamaseviciute, Tamasevicius, G Mykolaitis, S Bumeliene, and E Lindberg, *Nonlin. Anal. Mod. Cont.* **13** (2008) 241.
11. S Boccaletti, C Grebogi, YC Lai, H Mancini, and D Maza, *Phys. Rep*. **329** (2000) 103.
12. L M Pecora and T L Caroll, *Phys. Rev. Lett*. **64**, 8 (1990) 821.
13. S Rajasekar, S Murali, and M Lakshmanan, *Chaos Solitons & Fractals* **8**, 9 (1997) 1545.
14. J Wang, Z Duan, and L Huang, *Phys. Lett.* A **351** (2006) 143
15. B Liu, S Li, and Z Zheng, *Int. J. Nonlin. Sci*. **18** (2014) 40.
16. E Tamaseviciute, G Mykolaitis, and S Bumeliene, *Lith. J. Phys*. **47**, 3 (2007) 235.
17. K Briggs, *Math. Comp.* **57** (1991) 435.
18. A Wolf, J B Swift, H L Swinney, and J A Vastano, *Physica* D **16** (1985) 285.
19. V Gintautus, http: // guava. Physics. uiuc. edu/ ~nigel/courses/569/Essays_Spring2006/files/gintautas.pdf. (2006).
20. H Fotsin, S Bowong, and J Daafouz, *Chaos Solitons & Fractals* **26** (2005) 215.
21. V V Ashtakov, A N Silchenko, G I Strelkova, A V Shabunin, and V S Anishchenko, *J. Comm. Tech. Elec.* **41**, 14 (1996) 1323.